RSC Advances

PAPER

View Article Online
View Journal | View Issue

Cite this: *RSC Adv.*, 2014, **4**, 58260

Fabrication of a fayalite@C nanocomposite with superior lithium storage for lithium ion battery anodes†

Qingtang Zhang,*[a] Songwang Ge,[a] Hongtao Xue,[b] Xiaomei Wang,[b] Hanxue Sun[ab] and An Li*[a]

Received 11th September 2014
Accepted 30th October 2014

DOI: 10.1039/c4ra10206a

www.rsc.org/advances

A fayalite (α-Fe_2SiO_4)@C nanocomposite is successfully fabricated by a solid state reaction under the flow of nitrogen gas. The fayalite@C nanocomposite delivers a high specific capacity, excellent rate capability and good cycling performance as an anode material for lithium ion batteries (LIB). The initial discharge capacity and reversible charge capacity of the fayalite@C nanocomposite at 0.1 C reach up to 849.0 mA h g^{-1} and 514.5 mA h g^{-1}, respectively. The capacity ratio of 2 C/0.5 C is 90% indicating the excellent rate performance of the fayalite@C anode. In addition, the fayalite@C anode retains 84.3% of its original capacity after 100 cycles at 1 C. Taking into account the low cost and simple fabrication process, this kind of abundant mineral silicate has great potential for next generation LIB.

Introduction

Lithium ion batteries (LIB) have been extended to a wide range of applications in new energy vehicles, including hybrid electric vehicles, plug-in hybrid electric vehicles and electric vehicles, *etc.*, because of their excellent electrochemical properties such as high energy density, high power density, long cycling life, no memory effect and environmental benignity.[1–4] The development of high performance electrode materials is becoming essential to build advanced LIB for new energy vehicles. Among these high performance anode materials, mesoporous disordered carbon, transition metal oxides, tin based materials and silicon based materials have been exploited so far as promising candidates because of their much higher capacity than that of the commercial graphite anode (372 mA h g^{-1}). For example, mesoporous disordered carbon[5–7] has been reported to possess a high capacity of 500–1200 mA h g^{-1}, large rate performance and long cycling life due to its well-developed mesoporous structures which facilitate the penetration of the non-aqueous electrolyte and diffusion of the lithium ions. However, an obvious drawback of such materials lies in its huge initial irreversible capacity. The mechanism of lithium storage for the transitional metal oxides[8–11] based on the conversion reactions in which the metal oxides are reduced to transition metal nanodomains dispersed in Li_2O matrix upon lithiation and then are reversibly restored to the initial state after delithiation. High specific capacities up to 600–1000 mA h g^{-1} have been delivered for transitional metal oxides electrodes, but usually associated with drastic volume variation (up to 200%) in the most cases during charge–discharge cycles which in turn leads to short-term cycling stability. The storage of lithium for tin-based materials[12–14] and silicon based materials[15–17] mainly relies on the reversible alloying–dealloying reaction between the lithium and metal nanocrystals generated from the initial irreversible reduction of oxides. They exhibit high specific capacities of 600–3000 mA h g^{-1} but also suffer the drawbacks similar to that of the transitional metal oxides. Therefore, further development of novel, high performance anode materials should be of great importance for the next generation LIB.

In general, Li_2FeSiO_4, Li_2MnSiO_4 and $LiFePO_4$ have been widely used as cathode materials for LIB system. Recently, utilization of those cathode materials as anode materials has been received considerable attentions because their capacities are much higher for anode than for cathode. For instance, $LiFePO_4$ exhibits an initial capacity of 620 mA h g^{-1} and reversible capacity of 300 mA h g^{-1} when used as anode material, which is two times as that of cathode materials.[18] Similar results have also been found in Li_2MnSiO_4 and Li_2FeSiO_4 systems.[19,20] However, the lithium in the crystalline structure of these materials can not benefit to their capacities in the negative electrode. Along this line, the exploitation of lithium-free silicate may open a possibility for construction of novel anode materials for LIB.

Fe_2SiO_4 are important rock-forming silicates, which is a kind of low cost and the most abundant mineral in the earth's upper mantle. These compounds are important in geology, geophysics and materials science. Fe_2SiO_4 exist in two structures: the

[a]School of Petrochemical Engineering, Lanzhou University of Technology, Lanzhou 730050, China. E-mail: zhqt137@163.com; lian2010@lut.cn

[b]State Key Laboratory of Advanced Processing and Recycling of Non-ferrous Metals, Lanzhou 730050, China

† Electronic supplementary information (ESI) available. See DOI: 10.1039/c4ra10206a

olivine structure (orthorhombic α-Fe_2SiO_4 phase, usually named as fayalite) and the spinel structure (cubic γ-Fe_2SiO_4 phase).[21–25] Compared with γ-Fe_2SiO_4, fayalite is rather stable under ambient conditions and easy available from natural source. Recently, the preparation of fayalite nanocrystalline by simple roasting sol–gel precursor[26] or single-step mechanosynthesis[27] has been reported. However, employment of Fe_2SiO_4 as anode materials for LIB has never been reported to date, to the best of our knowledge. Taking into account of the similar structure of fayalite to Li_2FeSiO_4, we decided it may be used as novel anode materials. As a proof-of-concept study, here we reported for the first time the preparation of fayalite@C nanocomposite as anode for LIB as well as systematically investigation of their electrochemical properties. Taking advantages of high specific capacity, excellent rate capability, low cost and simple fabrication, fayalite may have great potentials as anode materials for advanced LIB. Meanwhile, the findings obtained from our study may also provide a new route to the rational design and fabrication of novel anode materials based on fayalite such as other metal ions doped or co-doped fayalite, porous or mesoporous fayalite, fayalite/C/carbon nanotubes, fayalite/C/reduced graphene oxide, and $LiFePO_4$ coated fayalite.

Experimental

Sample preparation

Nanocrystalline fayalite had been fabricated *via* single-step mechanosynthesis of the mixture of α-Fe_2O_3, Fe and SiO_2 reactants in a molar ratio of 2 : 2 : 3 by Šepelák *et al.*[27] Here, according to the solid state reaction of Li_2FeSiO_4/C,[28–32] fayalite@C composite was prepare by traditional solid state reaction from reactants such as nano SiO_2, $FeC_2O_4 \cdot 2H_2O$ and ammonium citrate. In a typical synthesis, a mixture of 0.02 mol nano SiO_2, 0.04 mol $FeC_2O_4 \cdot 2H_2O$ and 0.02 mol ammonium citrate was ball-milled in 20 ml ethanol for 2 hours. Then, the resulting mixture was dried at 80 °C in a vacuum drying oven for 6 hours. The dried mixture was afterwards transferred to a quartz boat and heated under a flow of N_2 gas. Firstly, the mixture was calcined at 350 °C for 3 h to pre-carbonize the ammonium citrate. Secondly, the mixture was kept at 700 °C for 6 h to obtain the fayalite@C nanocomposite.

Characterization

Fayalite@C nanocomposite was characterized by a field-emission scanning electron micro-scope (FESEM, JEOL, JSM-6701F), a transmission electron microscope (TEM, JEOL, JEM-2100F), and a powder X-ray diffraction (XRD, Rigaku RINT2000 X-ray Diffractometer, Cu K_α, $\lambda = 1.5406$ Å). An elemental analysis instrument (Elementar Analysensysteme GmbH) was also used to determine the actual carbon content of fayalite@C nanocomposite.

Coin type CR2032 cells were assembled to evaluate the electrochemical performance of fayalite@C nanocomposite. The cells all consists of a fayalite@C anode and a lithium metal counter electrode separated by a microporous polypropylene separator (Celgard 2400). The electrolyte was 1 mol L^{-1} $LiPF_6$ dissolved in a mixture of ethylene carbonate (EC), dimethyl carbonate (DMC) and ethyl-methyl carbonate (EMC) with a volume ratio of 1 : 1 : 1. The fayalite@C anode was prepared as follows. Firstly, 85 wt% fayalite@C nanocomposite, 5 wt% Super P carbon black and 10 wt% aqueous LA132 binder (Chengdu Indigo power sources Co., Ltd.) were homogeneously mixed in an agate mortar to fabricate slurry. Secondly, the slurry was spread onto a 9 μm copper foil and then split into flakes with a diameter of 12 mm. The assembled cells were cycled between 0 and 3 V (*vs.* Li^+/Li) at the room temperature (25 °C) using a CT2001A LAND battery testing system (Wuhan LAND Electronics Co., Ltd.). Cyclic voltammetry (CV) measurements were carried out on a ZF-100 electrochemical workstation (Shanghai Zhengfang Electronics Co., Ltd.).

Results and discussion

The crystalline structure of fayalite is orthorhombic with space group *Pbnm* (no. 62), which is shown in Fig. 1a. Fayalite@C nanocomposite was then determined by powder X-ray diffraction (XRD). As shown in Fig. 1b, typical α-Fe_2SiO_4 phase (JCPDS PDF 34-0178) was observed in the XRD pattern of fayalite@C nanocomposite. The XRD results are in good accordance with Šepelák's study.[27] A very weak peak of Fe was found in the patterns, indicating that small amount of Fe impurity exists in the nanocomposite. The small amount of Fe benefits to the electronic conductivity which in turn may lead to an improvement on the electrochemical performance of fayalite@C

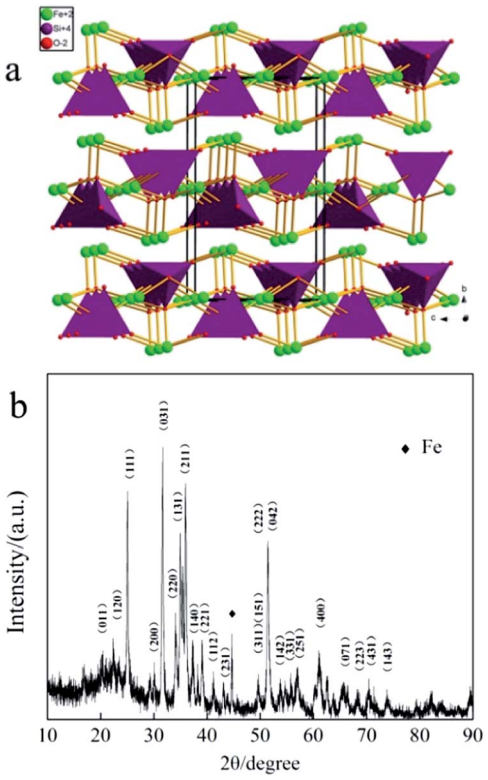

Fig. 1 (a) Crystal structure of orthorhombic fayalite. (b) XRD patterns of fayalite@C nanocomposite.

nanocomposite. There are no clear peaks of carbon indicating that the addition of carbon had no influence on the main reaction to form Fe_2SiO_4 crystal. And the *in situ* carbon coating can enhance the electronic conductivity of Fe_2SiO_4. In addition, the lithium can also be stored in the coated carbon and have been proved in previous studies.[6,7] Elemental analysis results further indicate that the actual carbon content of fayalite@C nanocomposite is 15.5%.

Fig. 2a shows the SEM image of fayalite@C nanocomposite which is consisted of nanoparticles. The particle sizes were analysed from the SEM image and the result is shown in Fig. 2b. The fayalite@C nanocomposite has a size within the range of 10 nm to 70 nm, mainly between 20 nm to 40 nm. The particle size of fayalite@C nanocomposite is roughly similar to that of raw materials nano SiO_2 (Fig. S1, (ESI†)). So, we can assume that the Fe^{2+} ions migrate into nano SiO_2 to form nano fayalite. Fig. 2c shows the SEM image of fayalite nanoparticle without *in situ* carbon coating. The particle sizes were analysed from the SEM image and the result is shown in Fig. 2d. The fayalite nanoparticle has a size within the range of 20 nm to 100 nm, mainly between 50 nm to 80 nm. The particle size of fayalite nanoparticle is obviously larger than that of fayalite@C nanocomposite. Therefore, the *in situ* carbon coating can hinder particle growth of Fe_2SiO_4 particle. Similar results have been proved by other groups in preparation of Li_2FeSiO_4/C nanocomposite.[28–32] Representative TEM micrographs of fayalite@C nanocomposite at low and high magnifications are shown in Fig. 2e and f, respectively. Nanoparticles can also be observed in the both images. The nanoparticles were found to be irregular shapes, consisting of an ordered region (crystalline inner core) surrounded/separated by a structurally disordered carbon surface shell/interface region. The HRTEM micrograph also shows lattice fringes. The electron diffraction pattern of the fayalite@C nanocomposite shows only spot patterns (Fig. 2f inset), which indicates the presence of fayalite crystallines. The energy-dispersive spectroscopy (EDS) measurement confirms that the co-existence of Fe, Si, C and O elements and the Fe : Si atomic ratio is 2 : 1 (Fig. S2, ESI†).

The specific capacity of fayalite@C anode was determined by the mass of fayalite@C nanocomposite. The discharge–charge voltage profiles of fayalite@C anode are shown in Fig. 3. The open-circuit voltage of the assembled cell was found to be about 3.23 V. High initial discharge (lithiation) and charge (delithiation) capacities of around 849.0 mA h g^{-1} and 514.5 mA h g^{-1} can be achieved, respectively. The 39.4% initial irreversible capacity loss is mainly attributed to the initial irreversible reduction on the electrode, electrolyte decomposition and inevitable formation of a solid electrolyte interface (SEI) layer and other irreversible processes such as irreversible formation of Li_2O and trapping of some lithium in the lattice, similar to most of common anode materials.[11,15–20] The value is distinctly lower than that of nitrogen-rich mesoporous carbon,[6] mesoporous carbon[7] and amorphous $CoSnO_3$@C nanoboxes,[11] indicating a good reversible lithium lithiation/delithiation property. The second discharge and charge capacities were measured to be 504.9 mA h g^{-1} and 489.5 mA h g^{-1}, respectively. The coulombic efficiency increases rapidly to 96.9% in the second cycle. This reversible capacity is considerably higher than the theoretical capacity of commercial graphite electrodes (372 mA h g^{-1}) and is competitive to mesoporous carbon[5,7] and amorphous $CoSnO_3$@C nanoboxes.[11] As shown in Fig. 3, a wide voltage plateau at about 0.8 V can be observed during the first

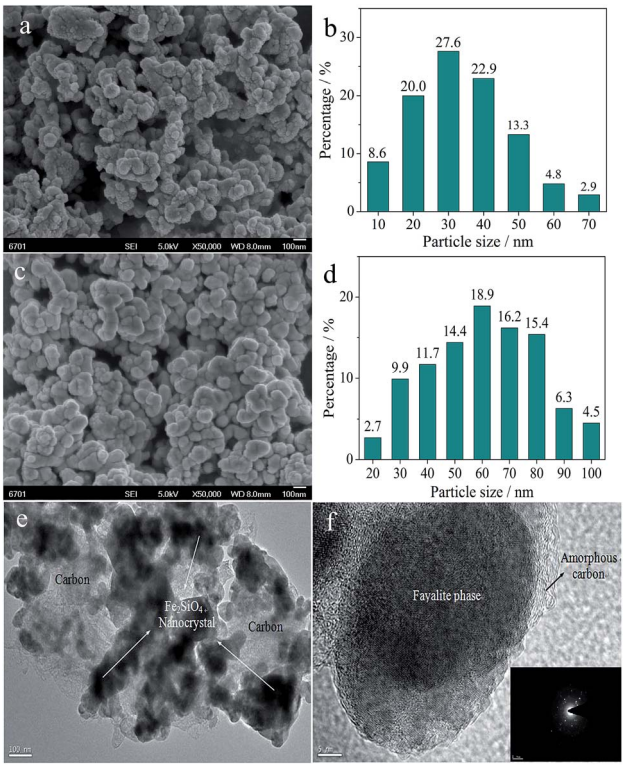

Fig. 2 (a) SEM image of fayalite@C nanocomposite, scale bar: 100 nm. (b) Particle size distributions of fayalite@C nanocomposite analysed from the SEM image. (c) SEM image of fayalite nanoparticle, scale bar: 100 nm. (d) Particle size distributions of fayalite nanoparticle analysed from the SEM image. (e) TEM micrographs of fayalite@C nanocomposite at low magnifications, scale bar: 100 nm. (f) TEM micrographs of fayalite@C nanocomposite at high magnifications, scale bar: 5 nm, inset is the SAED pattern of fayalite@C nanocomposite.

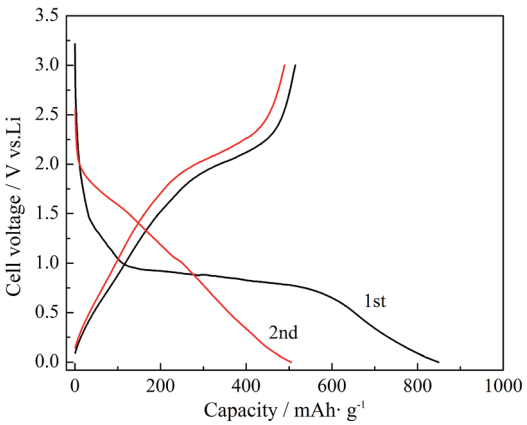

Fig. 3 Initial and second cycles of galvanostatic discharge–charge curves of fayalite@C anode.

discharge process which may be attributed to the initial reduction of Fe^{2+} to Fe^0 and the formation of the amorphous Li_2O.[20]

To confirm the structure change during the first discharge–charging process, the fresh fayalite@C anode and fayalite@C anode after the first discharge–charge process were determined by the *ex situ* XRD. As shown in Fig. 4, Fe_2SiO_4 crystal diffraction peaks are clearly observed in the fresh fayalite@C anode, while no Fe_2SiO_4 crystal diffraction peaks are detected in the fayalite@C anode after the first discharge–charge process. Cu diffraction peaks are attributed to the Cu current collector of the fayalite@C anode. The *ex situ* XRD results indicate an irreversible structure change that crystalline fayalite turns to the mixture of amorphous FeO, Li_2O and SiO_2 in the first discharge–charge cycle. Fig. 3 reveals that second charge capacity is very near to the initial charge capacity, implying reversible lithium storage capability of those materials. In other words, the material is stable in the following discharge–charge tests.

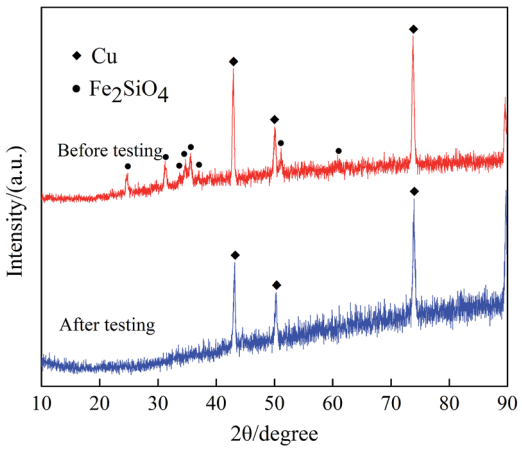

Fig. 4 *Ex situ* XRD patterns of the fresh fayalite@C anode and the fayalite@C anode after the first discharge–charge process.

The CV of the fresh cells was tested to evaluate the anodic and cathodic properties of the fayalite@C anode. As shown in Fig. 5a, the reduction peak of CV curves at a high scan rate of 0.5 mV S^{-1} is about 0.2 V. However, as shown in Fig. 5b, the reduction peak of CV curves at a very low scan rate of 0.02 mV S^{-1} is about 0.66 V. The phenomenon reveals that the electronic conductivity of fresh electrode is very poor. In the first anodic scan, a broad peak between 1.5 and 2.5 V can be observed. Xu *et al.* thought the peak is attributed to a change of iron oxidation state in two steps (Fe^0 to Fe^{2+} at *ca.* 1.6 V and Fe^{2+} to Fe^{3+} at *ca.* 2.0 V).[20] However, the second cathodic scan is quite different from the first one, in which the reduction peaks become weaker, and shift to 1.5 V (a broad peak between 1.0 and 2.0 V), corresponding to the reverse reaction. The redox peaks of second scan at scan rate of 0.5 mV S^{-1} is similar to that of 0.02 mV S^{-1}, indicating the electronic conductivity of electrode becomes much higher and the electrochemical reversibility of the electrodes is gradually built after the initial cycle, in which fayalite

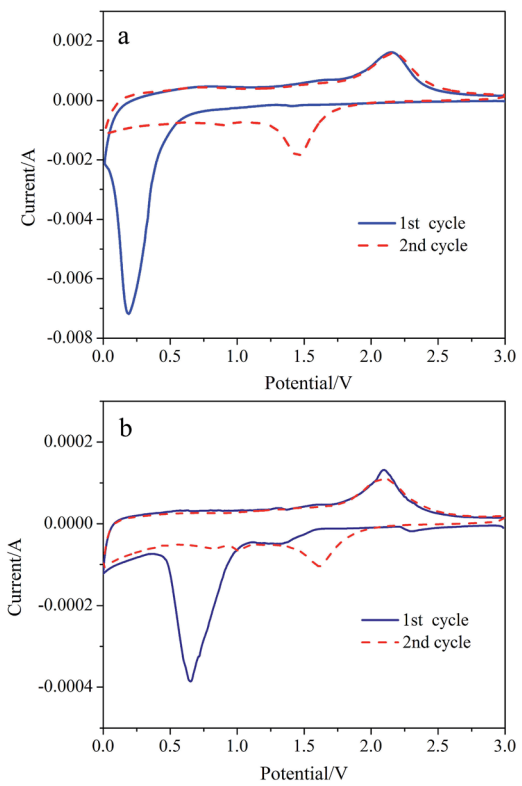

Fig. 5 (a) CV curves of fayalite@C anode at a scan rate of 0.5 mV S^{-1}. (b) CV curves of fayalite@C anode at a scan rate of 0.02 mV S^{-1}.

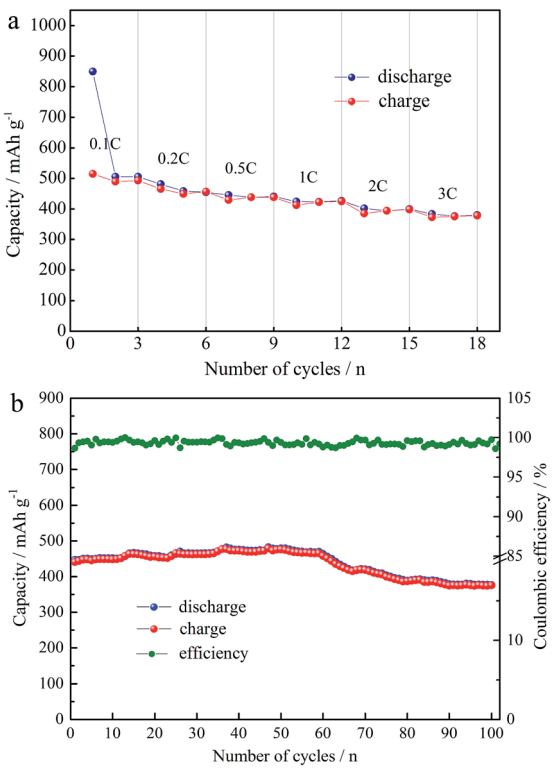

Fig. 6 (a) Specific capacity of the fayalite@C anode as a function of the cycling rate C. (b) Cycling performance of the fayalite@C anode at a charge–discharge rate of 1 C for 100 cycles.

crystals with poor electronic conductivity are destroyed. No Si-alloying redox peaks are detected. Therefore, the $Fe^{3+}/Fe^{2+}/Fe^{0}$ redox may be responsive to the high capacity of fayalite@C anode.

In order to fully estimate the electrochemical performance of fayalite@C anode, the consecutive cycling behaviors at enhanced discharge–charge current rates ranging from 0.1 C to 3 C are shown in Fig. 6a. The fayalite@C anode exhibits good rate performance and good reversible capacities of 514.5 mA h g^{-1}, 465.3 mA h g^{-1}, 428.7 mA h g^{-1}, 412.6 mA h g^{-1}, 384.5 mA h g^{-1} and 372.4 mA h g^{-1} at the current rates of 0.1 C, 0.2 C, 0.5 C, 1 C, 2 C and 3 C were obtained, respectively. The capacity ratio of 2 C/0.5 C is 90% indicating the excellent rate performance of the fayalite@C anode. After the rate performance tests, the fayalite@C anode was further discharge–charged at the current rate of 1 C for 100 cycles to evaluate the cycling stability of the fayalite@C nanocomposite. The results are shown in Fig. 6b. The first and 100th charge capacities at 1 C are measured to be 447.0 mA h g^{-1} and 376.7 mA h g^{-1}, respectively. The capacity retention ratio of the fayalite@C anode is 84.3%, which indicates good cycling performance of the fayalite@C anode. In addition, all the coulombic efficiency of the 100 cycles at the current rate of 1 C is above 98.5%.

Conclusions

In summary, we have prepared and investigated the fayalite@C nanocomposite for highly reversible lithium storage. This fayalite@C anode shows high reversible lithium storage capacity, excellent rate performance and cycling performance, which is quite different from the common anode materials. In addition, Fe_2SiO_4 are important rock-forming silicates, the most abundant mineral in the earth's upper mantle. When evaluated as an anode material for LIB, this kind of silicates may hold great promise for the development of low price and high-performance LIB for new energy vehicles.

Acknowledgements

This research was supported by the National Nature Science Foundation of China (no. 21466020, 51263012, 51262019), Gansu Provincial Science Fund for Distinguished Young Scholars (Grant no. 1308RJDA012). We also thank Dr Junling Song for structure simulation.

Notes and references

1 H. G. Jung, M. W. Jang, J. Hassoun, Y. K. Sun and B. Scrosati, *Nat. Commun.*, 2011, **2**, 516–520.
2 V. Etacheri, R. Marom, R. Elazari, G. Salitra and D. Aurbach, *Energy Environ. Sci.*, 2011, **4**, 3243–3262.
3 J. B. Goodenough and K. S. Park, *J. Am. Chem. Soc.*, 2013, **135**, 1167–1176.
4 B. Scrosati, J. Hassoun and Y. K. Sun, *Energy Environ. Sci.*, 2011, **4**, 3287–3292.
5 Q. Zhang, S. Ge, X. Wang, H. Sun, Z. Zhu, W. Liang and A. Li, *RSC Adv.*, 2014, **4**, 41649–41653.
6 Y. Mao, H. Duan, B. Xu, L. Zhang, Y. S. Hu, C. C. Zhao, Z. X. Wang, L. Q. Chen and Y. S. Yang, *Energy Environ. Sci.*, 2012, **4**, 7950–7955.
7 B. Xu, L. Shi, X. W. Guo, L. Peng, Z. X. Wang, S. Chen, G. P. Cao, F. Wu and Y. S. Yang, *Electrochim. Acta*, 2011, **56**, 6464–6468.
8 H. S. Lim, B. Y. Jung, Y. K. Sun and K. D. Suh, *Electrochim. Acta*, 2012, **75**, 123–130.
9 Y. J. Mai, X. H. Xia, R. Chen, C. D. Gu, X. L. Wang and J. P. Tu, *Electrochim. Acta*, 2012, **67**, 73–78.
10 J. Z. Wang, N. Du, H. Wu, H. Zhang, J. X. Yu and D. R. Yang, *J. Power Sources*, 2013, **222**, 32–37.
11 Z. Y. Wang, Z. C. Wang, W. T. Liu, W. Xiao and X. W. Lou, *Energy Environ. Sci.*, 2013, **6**, 87–91.
12 J. Z. Chen, L. Yang, S. H. Fang and S. I. Hirano, *J. Power Sources*, 2012, **209**, 204–208.
13 W. S. Kim, Y. Hwa, J. H. Jeun, H. J. Sohn and S. H. Hong, *J. Power Sources*, 2013, **225**, 108–112.
14 X. W. Guo, X. P. Fang, Y. Sun, L. Y. Shen, Z. X. Wang and L. Q. Chen, *J. Power Sources*, 2013, **226**, 75–81.
15 T. Kim, Y. H. Mo, K. S. Nahm and S. M. Oh, *J. Power Sources*, 2006, **162**, 1275–1281.
16 H. C. Tao, L. Z. Fan and X. H. Qu, *Electrochim. Acta*, 2012, **71**, 194–200.
17 K. Kang, K. Song, H. Heo, S. Yoo, G. S. Kim, G. Lee, Y. M. Kang and M. H. Jo, *Chem. Sci.*, 2011, **2**, 1090–1093.
18 N. Kalaiselvi, C. H. Doh, C. W. Park, S. I. Moon and M. S. Yun, *Electrochem. Commun.*, 2004, **6**, 1110–1113.
19 V. Aravindan, K. Karthikeyan, S. Amaresh, H. S. Kim, D. R. Chang and Y. S. Lee, *Ionics*, 2011, **7**, 3–6.
20 Y. Xu, Y. Z. Li, S. Q. Liu, H. L. Li and Y. N. Liu, *J. Power Sources*, 2012, **220**, 103–107.
21 T. Yagi, F. Marumo and S. Akimoto, *Am. Mineral.*, 1974, **59**, 486–490.
22 U. Brinkmann and W. Laqua, *Phys. Chem. Miner.*, 1985, **12**, 283–290.
23 T. Yamanaka, *Phys. Chem. Miner.*, 1986, **13**, 227–232.
24 W. Yong, E. Dachs, A. C. Withers and E. J. Essene, *Phys. Chem. Miner.*, 2007, **34**, 121–127.
25 M. Koch-müller, D. Rhede, R. Schulz and R. Wirth, *Phys. Chem. Miner.*, 2009, **36**, 329–341.
26 M. T. DeAngelis, A. J. Rondinone, M. D. Pawel, T. C. Labotka and L. M. Anovitz, *Am. Mineral.*, 2012, **97**, 653–656.
27 V. Šepelák, M. Myndyk, M. Fabián, K. L. D. Silva, A. Feldhoff, D. Menzel, M. Ghafari, H. Hahn, P. Heitjans and K. D. Becker, *Chem. Commun.*, 2012, **48**, 11121–11123.
28 X. B. Huang, X. Li, H. Y. Wang, Z. L. Pan, M. L. Qu and Z. L. Yu, *Solid State Ionics*, 2010, **181**, 1451–1455.
29 X. Wang, C. Qing, Q. Zhang, W. Fang, X. Huang, B. Yang and J. Cui, *Electrochim. Acta*, 2014, **134**, 371–376.
30 J. Yia, M. Y. Hou, H. L. Bao, C. X. Wang, J. Q. Wang and Y. Y. Xia, *Electrochim. Acta*, 2014, **133**, 564–569.
31 J. Cui, C. Qing, Q. Zhang, C. Su, X. Wang, B. Yang and X. Huang, *Ionics*, 2014, **20**, 23–28.
32 W. Chen, M. Lan, D. Zhu, C. Wang, S. Xue, C. Yang, Z. Li, J. Zhang and L. Mi, *RSC Adv.*, 2013, **3**, 408–412.

